PERGAMON

Progress in Materials Science 46 (2001) 249–271

Progress in Materials Science

www.elsevier.com/locate/pmatsci

Mechanics-based scaling laws for the durability of thermal barrier coatings

A.G. Evans [a,*], M.Y. He [b], J.W. Hutchinson [c]

[a] *Princeton Materials Institute, Princeton University, Princeton, NJ 08540, USA*
[b] *Materials Department, University of California at Santa Barbara, CA 91360, USA*
[c] *Division of Engineering and Applied Science, Harvard University, Cambridge, MA 02138, USA*

Abstract

The durability of thermal barrier systems is governed by a sequence of crack nucleation, propagation and coalescence events that accumulate prior to final failure by large scale buckling and spalling. This sequence is governed by the σ_{zz} stresses that develop normal to the substrate, around imperfections, as the thermally grown oxide (TGO) thickens. Their effect is manifest in the stress intensity factor, K, caused by the σ_{zz} stresses acting on cracks emanating from them. In turn, these events are governed by scaling laws, ascribed to non-dimensional groups governing σ_{zz} and K. In this article the basic scaling relations are identified and used to gain some understanding of the relative importance of the various mechanisms that arise for application scenarios with minimal thermal cycling. These mechanisms are based on stresses that develop because of TGO growth strains in combination with thermal expansion misfit. The results are used to identify a critical TGO thickness at failure and express it in terms of the governing material variables. The changes in behavior that arise upon extensive thermal cycling, in the presence of TGO ratcheting, are elaborated elsewhere.

Contents

* Corresponding author.
E-mail address: anevans@princeton.edu (A.G. Evans).

0079-6425/01/$ - see front matter
PII: S0079-6425(00)00007-4

1. Introduction

Thermal barrier coatings (TBCs) are widely used in turbines for propulsion and power generation [1–6]. They comprise thermally insulating materials having sufficient thickness and durability that they can sustain an appreciable temperature difference between the load bearing alloy and the surface. The benefit of these coatings results from their ability to sustain high thermal gradients in the presence of adequate back-side cooling. Lowering the temperature of the metal substrate prolongs the life of the component. Successful implementation has required comprehensive testing protocols, facilitated by engineering models [7–9]. Expanded application to more demanding scenarios requires that their basic thermo-mechanical characteristics be understood and quantified. This need motivates the analysis presented in this article. There are *four primary constituents* in a thermal protection system (Fig. 1). They comprise (i) the TBC itself, (ii) an aluminum containing bond coat (BC) between the substrate and the TBC, (iii) a thermally grown oxide (TGO), predominantly alumina, that forms between the TBC and the BC, and (iv) the superalloy substrate. The TBC is the insulator, the BC provides the oxidation protection and the alloy sustains the structural loads. The TGO is a reaction product. Each of these elements is dynamic and all interact to control the performance and durability. The thermal barrier coating is an insulating, "strain tolerant" oxide. Zirconia has emerged as the preferred material, stabilized into its cubic/tetragonal forms by the addition of yttria in solid solution. This material has low thermal conductivity with minimal temperature sensitivity [10]. Strain tolerance is designed into the material to avoid instantaneous delamination from the thermal expansion misfit with the substrate [1,4,6,7]. The deposition conditions are designed to create multi-scale porosity that provides the requisite strain tolerance and also reduces the thermal conductivity. The bond coat alloy is designed as a local Al reservoir, enabling α-alumina to form in preference to other oxides [11–13]. Alumina is the preferred thermally grown oxide because of its low oxygen diffusivity and superior adherence. Bond coats are in two categories.

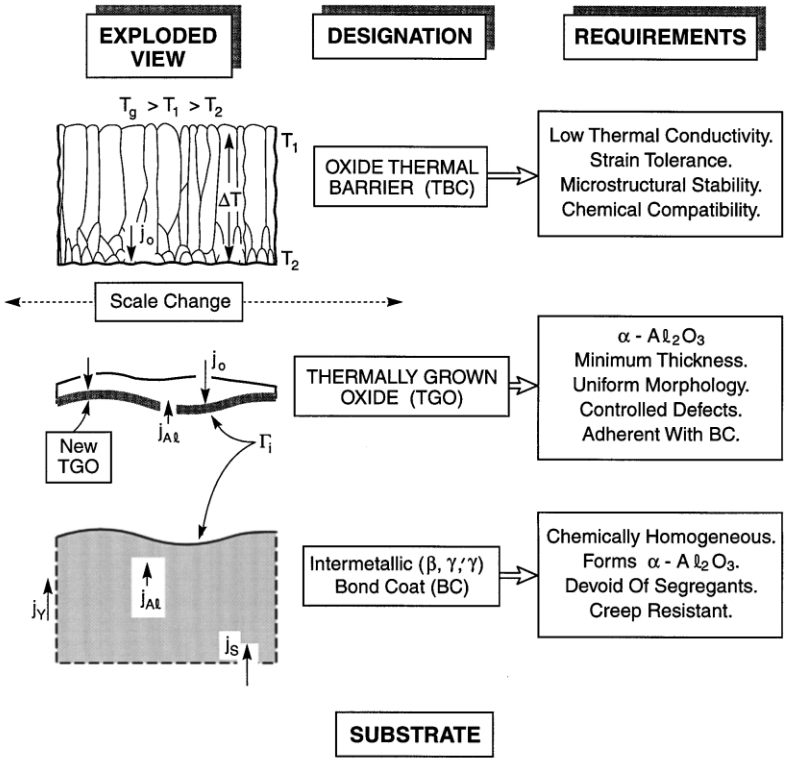

Fig. 1. An exploded view of the four major constituents of a thermal barrier system.

One is based on the NiCoCrAlY system. Such coatings are generally two phase (γ'-Ni_3Al with β-NiAl). The Y is added at low concentrations to improve the adhesion of the TGO, by acting as a solid state gettering site for S [14–16]. The second category consists of a Pt-aluminide. These coatings are typically single-phase-β, with Pt in solid solution [12]. The TGO layer, which forms predominantly at the highest temperature in the thermal cycle, develops extremely large residual compressions at ambient (3–6GPa) [17–19]. These arise primarily on cooling, because of its thermal expansion misfit with the substrate (Table 1). Smaller, yet significant, stresses also arise during TGO growth [12,18]. Though thin (about 10 μm), the strain misfit in the TGO motivates the failure mechanisms to be addressed in this article. In such cases, eventual failure is associated with the appearance of large-scale buckles (LSB), several mm in diameter [20,21]. Spalled areas may also appear at free edges [21].

The approach taken is to use basic failure-related observations to guide the development of mechanics-based scaling laws. Two general observations provide benchmarks. One finding is that failure of any specific TBC system is correlated with the thickness, h, of the thermally grown oxide [1,6,8,22]. There is also compelling evidence that failure is connected with the presence of imperfections between the

Table 1
Summary of material properties

1. *TBC (ZrO_2/Y_2O_3)*	
Thermal expansion coefficient, α_{tbc} (C^{-1} ppm)	11–13
Young's modulus, E_{tbc} (GPa)	0–100
Delamination toughness, Γ_{tbc} ($J\ m^{-2}$)	1–100
2. *TGO (α-Al_2O_3)*	
Young's modulus, E_o (GPa)	350–400
Growth stress, σ^g_{xx} (GPa)	0–1
Misfit compression, σ_o (GPa)	3–4
Mode I fracture toughness, Γ_o ($J\ m^{-2}$)	20
Thermal expansion coefficient, α_o (C^{-1} ppm)	8–9
3. *Interface (α-Al_2O_3/bond coat)*	
Mode 1 adhesion energy, Γ_1^o ($J\ m^{-2}$)	
Segregated	5–20
Clean	>100
4. *Bond coat*	
Young's modulus, E_s (GPa)	200
Yield strength (ambient temperature), σ_Y (MPa)	300–900
Thermal expansion coefficient, α_s (C^{-1} ppm)	13–16
5. *Substrate (Ni-alloy)*	
Thermal expansion coefficient, α_s (C^{-1} ppm)	13–16

TBC and the bond coat [23–26]. The most ubiquitous comprise undulations in the bond coat surface (Fig. 2). Stress development around such imperfections, as the TGO thickens, becomes a basic input to failure laws. Analysis of energy release rates for cracks emanating from these imperfections, followed by an assessment of their coalescence, completes this description.

With minimal thermal cycling, the sources of stress are those formed upon TGO growth, followed by the changes that happen because of thermal expansion misfit on cooling to ambient. Extensive thermal cycling introduces a different set of stresses, caused by phenomena such as ratcheting, which will be analyzed separately [27]. To address failure, the zones that experience tensile stress normal to the interface are most important, since these stresses are responsible for nucleating and propagating delaminations. Before attempting analyses that include the full geometric complexity of actual imperfections (Fig. 2), insights about the signs and relative magnitudes of the stresses and the energy release rates are obtained by analyzing spherical configurations subject to misfit strains. Subsequently, numerical results are obtained for configurations more similar to those found in actual TBCs.

2. Analytical assessments

The stresses induced by TGO growth differ from those caused by expansion misfit because of the differing nature of the associated "transformation" strains. Thermal

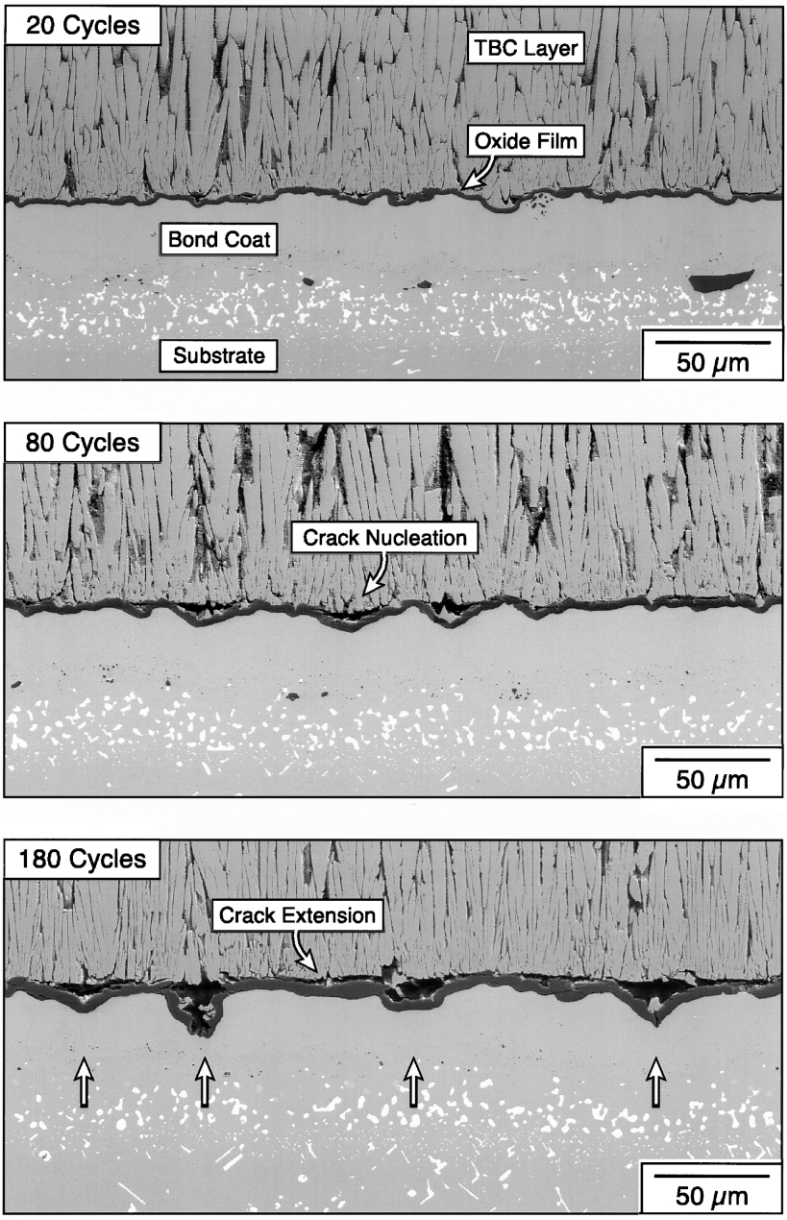

(a)

Fig. 2. Undulation imperfections found in typical thermal barrier systems. (a) A TBC made by electron beam physical vapor deposition (EB-PVD) on a Pt-aluminide bond coat. This sequence shows both the growth of the TGO as the system cycles and the growth of imperfections by ratcheting (courtesy D. Mumm). (b) A plasma sprayed TBC on a CoNiCrAlY bond coat. This sequence shows the growth of the TGO with exposure time and the evolution of cracks at imperfections. In the final image, the cracks have coalesced through the TGO (courtesy A. Rabiei).

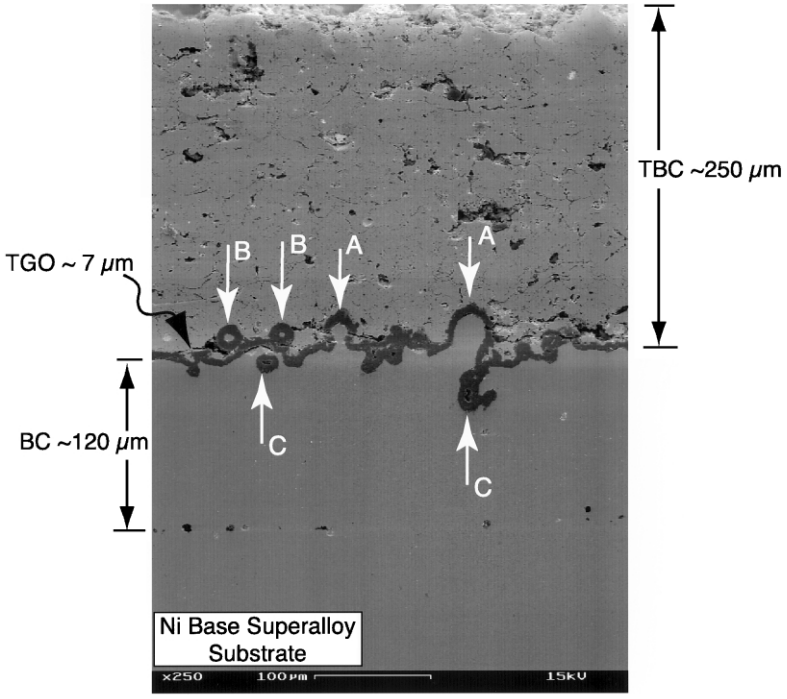

(b)

Fig. 2 (*continued*)

contraction is essentially isotropic with misfit strains of order 10^{-2} (Table 1). Conversely, the growth strains are anisotropic, partitioning differently normal and parallel to the interface [25,28,29]. The misfit is predominantly along the normal, because most of the new oxide forms at the TGO/bond coat interface (Fig. 3) [25]. While the strains are much larger than those caused by thermal expansion, the stresses need not be larger since they are partially redistributed by creep in the bond coat as well as the TGO itself.

Preliminary results for the stresses in the TBC, TGO and bond coat are estimated by considering imperfections having spherical symmetry (Fig. 4). There are two obvious limitations of this geometry. (i) The stress in the bond coat is hydrostatic and consequently, suppresses the yield and creep expected in more realistic configurations. (ii) The amelioration of the stresses enabled by the rigid body displacement of the TBC above an undulation is not allowed in the spherical model. The import of these deficiencies will be addressed in the second, numerical stage of the analysis, conducted for realistic imperfection morphologies. It will be demonstrated by such calculations that the stresses in the TGO and TBC near the apex of the imperfections are reasonably well-ordered in sign and magnitude by the analytical model. Solutions are first presented for a case wherein the three materials have the same elastic properties (Young's modulus, E, and Poisson's ratio, ν). Elastic mismatch can

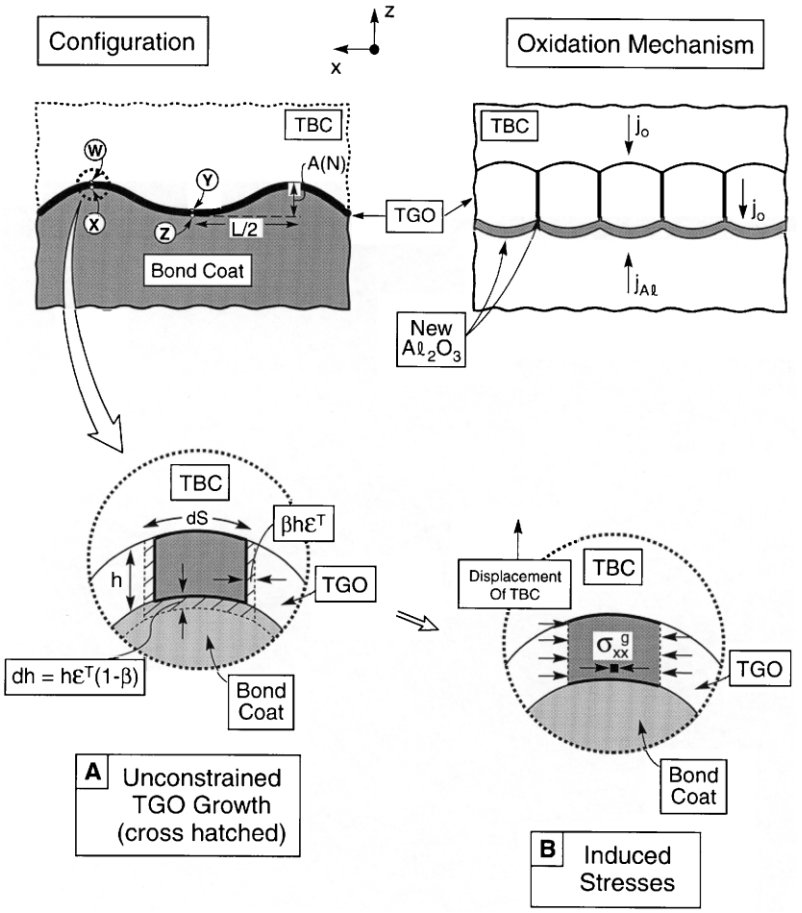

Fig. 3. Schematics of the configurations and the TGO growth mechanisms. The lower illustrations indicate phenomena that govern the growth stresses when anion-controlled.

also be taken into account, but the formulas become too lengthy to reveal trends. The effects of elastic mismatch are assessed later.

2.1. Thermal expansion misfit stresses

The elastic solutions for thermal expansion misfit in a tri-material system with spherical symmetry (Fig. 3) can be readily derived. The most straight forward approach employs the "Eshelby" protocol [30] of allowing the strains to occur unconstrained and imposing the tractions needed to assure displacement and traction continuity (Fig. 4**A**). The case of interest is one wherein the TGO (2) has the lowest thermal expansion coefficient, α_o, the substrate (3) the largest, α_s, and the TBC (1) the intermediate, α_{tbc}. The outer region (1) representing the TBC extends to

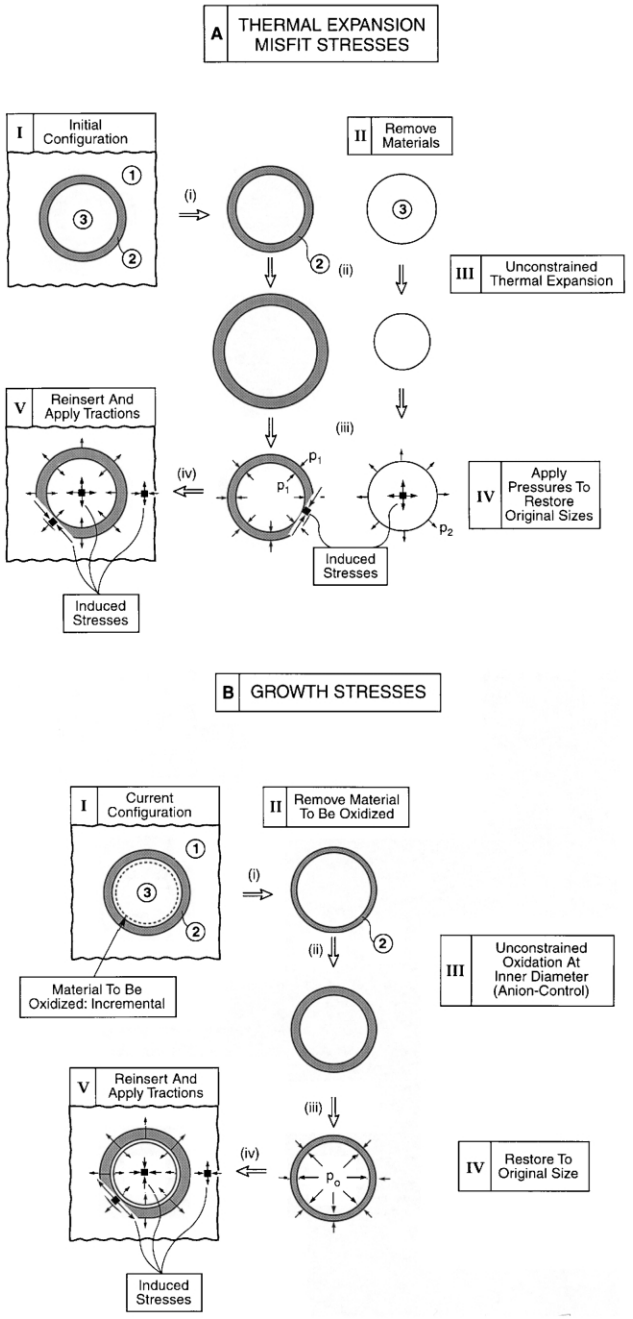

Fig. 4. The stresses that develop around spherical imperfections illustrated by using the ''Eshelby'' procedure [30]. (**A**) Thermal expansion misfit, (**B**) anion-controlled TGO growth. The three regions are as follows: (1) is the TBC, (2) is the TGO and (3) is a bond coat/substrate combination.

infinity. Throughout this section, the meridional stress, $\sigma_{\varphi\varphi}$, and the hoop stress, $\sigma_{\theta\theta}$, are equal by spherical symmetry. The stresses in the substrate/bond coat are:

$$\sigma_{rr} = \sigma_{\theta\theta} = \Lambda(\alpha_{tbc} - \alpha_s) \tag{1a}$$

where

$$\Lambda = 4\kappa\mu\Delta T/[\kappa + 4\mu/3], \quad \mu = E/[2(1+\nu)], \quad \kappa = E/[3(1-2\nu)]$$

and ΔT is the cooling range (negative in sign). Accordingly, the bond coat is in a state of hydrostatic tension, independent of α_o. The stresses in the TGO are:

$$\sigma_{rr} = \Lambda\{\alpha_{tbc} - \alpha_o - (\alpha_s - \alpha_o)[(R-h)/r]^3\}$$
$$\sigma_{\theta\theta} = \Lambda\left\{\alpha_{tbc} - \alpha_o + \frac{1}{2}(\alpha_s - \alpha_o)[(R-h)/r]^3\right\} \tag{1b}$$

where $2R$ is the diameter of the imperfection and h is the TGO thickness. Note that since, $\alpha_s > \alpha_{tbc} > \alpha_o$, the TGO is always in hoop compression and the interface between the substrate and the TGO is in radial tension. The stresses in the TBC are:

$$\sigma_{rr} = -2\sigma_{\theta\theta} = -\Lambda\{\alpha_o - \alpha_{tbc} + (\alpha_s - \alpha_o)(1 - h/R)^3\}(R/r)^3 \tag{1c}$$

In this case, the sign of the stresses depends on the relative TGO thickness, h/R. When the TGO is thin, the second term in the parenthesis dominates and the TBC is in radial compression. However, above a critical TGO thickness, radial tension develops. This thickness, h_*, is given by:

$$h_*/R = 1 - [(\alpha_{tbc} - \alpha_o)/(\alpha_s - \alpha_o)]^{1/3} \tag{2}$$

The hoop tension in the TBC and the radial tension at the interface have particular relevance, as discussed later.

Results for undulations in the TGO, absent the TBC, provide some ancillary insights. The stresses along the interface can be non-dimensionalized using [31]:

$$\sigma_{ij}/(\sigma_o A/L) = H_{ij}(h/L, A/h, x/L) \tag{3a}$$

where A and L are defined in Fig. 5 and σ_o is the misfit stress for a planar surface given by:

$$\sigma_o = E(\alpha_o - \alpha_s)\Delta T/(1-\nu) \tag{3b}$$

The functions H_{ij} have been computed with a finite element representation and are plotted in Fig. 5. Consistent with the results for the spherical imperfection, tensile stresses arise normal to the interface at the peaks in the undulations. These can be large enough to cause interface separation [32,33]. However, contrary to the solutions

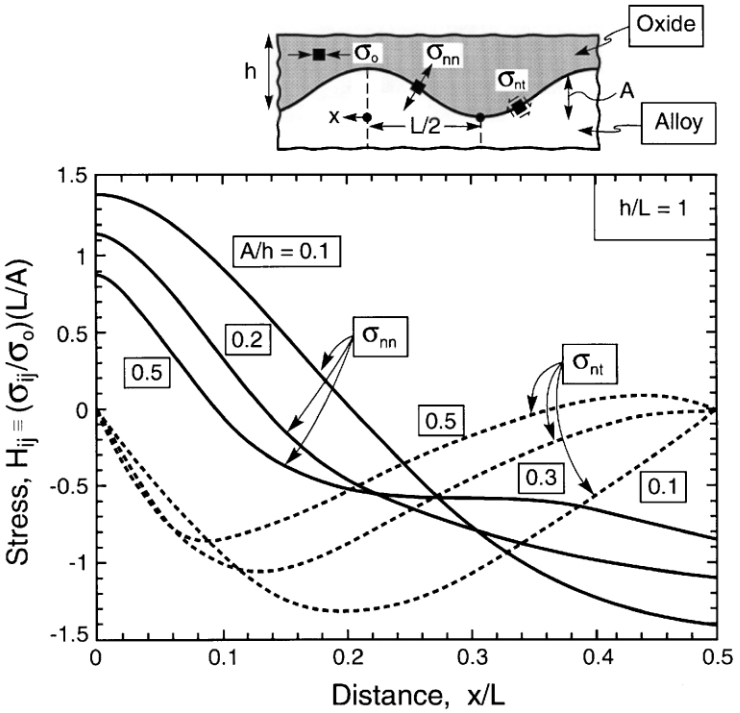

Fig. 5. Redistribution of thermal expansion misfit stress attributed to the presence of undulations. The stress σ_{nn} is that normal to the interface while σ_{nt} is the shear stress.

for the spherical geometry, shear stresses are induced in the bond coat at the sides of the imperfection that promote yielding and creep [31].

2.2. Oxide growth: intrinsic stresses

The stresses induced by TGO growth and thermal mismatch differ because the former occurs predominately at one of the interfaces (Figs. 3 and 4**B**) rather than uniformly throughout the TGO layer (Fig. 4**A**) [28,32]. For anion-control, growth is governed by inward diffusion of oxygen. It occurs at the interface where the bond coat is consumed (Fig. 3). For cation-control, the new oxide forms at the TGO/TBC interface, through the outward diffusion of Al (as well as Ni, Cr, etc.) [29]. The bond coat consumption still occurs at the inner interface. The former has been considered most relevant to α-alumina formation [11–16, 28]. The stresses within the TGO depend on the initial hoop stress component, $\sigma^i_{\theta\theta}$, generated at the instant of growth: an unknown quantity for most systems. The hoop stress distribution within the TGO will generally be different for the two growth processes.

The stresses due to growth of the TGO are determined upon neglecting creep and plasticity (see Section 2.3 for a discussion of the effect of creep in the spherical model). The calculation invokes small elastic strains and deformations. The stresses

for anion-control are obtained by an incremental process, wherein new TGO, thickness dh, is added at the TGO/bond coat interface. The ratio of new TGO volume to consumed bond coat volume is taken to be m. Thus, the net thickness of new material inserted is: $[(m-1)/m]\mathrm{d}h$. Each increment of new TGO is added at the current outer radius of the bond coat. Starting at $h=0$, the incremental expressions for the stresses are integrated to TGO thickness h. To be consistent with the small strain assumption, the analysis is limited to small values of h/R (e.g. no more than about 1/10), and the following results for the stresses have been expressed to lowest order in h/R. Within the bond coat,

$$\sigma_{rr} = \sigma_{\theta\theta} = -\frac{2E(m-1)}{3(1-\nu)m}\left(\frac{h}{R}\right) \tag{4a}$$

In the TBC, $r \geqslant R$,

$$\sigma_{rr} = -2\sigma_{\theta\theta} = -\frac{2E(m-1)}{3(1-\nu)m}\left(\frac{h}{R}\right)\left(\frac{R}{r}\right)^3 \tag{4b}$$

and within the TGO, $R-h \leqslant r \leqslant R$,

$$\sigma_{rr} = -\frac{2E(m-1)}{3(1-\nu)m}\frac{h}{R}$$
$$\sigma_{\theta\theta} = \sigma^{i}_{\theta\theta} + \frac{E(m-1)}{3(1-\nu)m}\left[\frac{r}{R} - \left(1-\frac{h}{R}\right)\right] \tag{4c}$$

For integration of the stress increments in the TGO, the only indeterminacy is the initial hoop stress at the growth interface, $\sigma^{i}_{\theta\theta}$, which can be prescribed arbitrarily. This initial value is included in the second of (4c), where its effect on the evolving hoop stress in the TGO becomes apparent. Otherwise, $\sigma^{i}_{\theta\theta}$ has no influence on the stresses in either the TBC or the bond coat. These results have the following features. The TBC is in radial compression and hoop tension, with radial compression in the TGO. These stresses increase as the TGO thickens. The hoop stress in the TGO is $\sigma^{i}_{\theta\theta}$ at the growth interface and $\sigma^{i}_{\theta\theta} + E(m-1)h/[3(1-\nu)mR]$ at the TGO/TBC interface. Thus, for example, if $\sigma^{i}_{\theta\theta} \cong 0$, the hoop stress throughout the TGO will be tensile. If $\sigma^{i}_{\theta\theta}$ is compressive, a tensile stress will develop at some stage in the outer portion of the TGO as it thickens.

The same steps can be carried out for cation-controlled growth wherein TGO growth occurs at the TGO/TBC interface and the bond coat is consumed at the inner TGO interface. Under the same small strain assumptions made above, the stresses in the bond coat and in the TBC remain the same, i.e. (4a) and (4b), respectively, and the radial stress in the TGO is still given by (4c). The only difference is in the distribution of the hoop stress within the TGO ($R-h < r < R$):

$$\sigma_{\theta\theta} = \sigma^{i}_{\theta\theta} - \frac{9E}{4(1-\nu)}\left(1-\frac{r}{R}\right), \tag{5}$$

Should $\sigma^{i}_{\theta\theta} \cong 0$, this stress will be compressive. Note that cation-controlled growth produces stress within the TGO even if there is no net volume change in the creation of the TGO ($m = 1$). This is a consequence of the transfer of material volume from the inner interface to the outer interface.

Subject to the simplifications used in the model, the stress magnitudes can now be compared. The growth stresses scale with $[Em/(m-1)](h/R)$, while the thermal stresses scale as $E\Delta\alpha\Delta T$. Evaluation for material properties representative of thermal barrier systems (Table 1), with $\Delta T = 1000^{\circ}\mathrm{C}$ and $h/R = 0.1$, indicates that TGO growth produces stresses on the order of several GPa in the TBC and tens of GPa in the TGO and bond coat. In practice, the low modulus of the TBC would partially alleviate these stresses. Thermal mismatch stresses are considerably less, on the order of several hundred MPa in the TBC and several GPa in the TGO and bond coat. The large stresses in the bond coat/substrate (region 3 in Fig. 4) are hydrostatic (a consequence of the spherical geometry), and will almost certainly relaxed by creep in the more realistic imperfection geometries discussed in Section 3. Moreover, the stresses in the TGO will be redistributed by internal creep. Nevertheless, the inference to be drawn from the above scaling is that the stresses induced by TGO growth predominate over those caused by expansion misfit. The tensile hoop stresses in the TBC are particularly relevant since they can lead to cracks spreading from the imperfection, as will be demonstrated in Section 2.4.

2.3. Role of TGO creep in redistributing stress in bond coat and TBC

A simple result based on the spherical model sheds considerable light on the extent which creep in the TGO (the most creep prone of the three materials [34–37]) is likely to produce stress redistribution in the TBC in the vicinity of the imperfection. Continue to ignore moduli differences among the three materials. Suppose the bond coat occupies the region, $r \leqslant R_s$; the TGO occupies $R_s \leqslant r \leqslant R$; and the TBC occupies $r \geqslant R$. Further, suppose creep occurs within the TGO such that the creep strain distribution is:

$$\varepsilon^{c}_{rr} = \varepsilon^{c}(r), \quad \varepsilon^{c}_{\theta\theta} = \varepsilon^{c}_{\varphi\varphi} = -\frac{1}{2}\varepsilon^{c}(r), \qquad (R_s \leqslant r \leqslant R) \tag{8}$$

The stress changes in the three regions, $\Delta\sigma_{ij}$, due to this creep can be obtained in closed form. In particular, the radial stress change acting on the TGO/TBC interface at $r = R$ is given by:

$$\Delta\sigma_{rr}(R) = 6\mu\left\{\int_{R_s}^{R}\left[r^{-1}\varepsilon^{c}(r) - R^{-3}r^{2}\left(\varepsilon^{c}(r) + \int_{R_s}^{r}\eta^{-1}\varepsilon^{c}(\eta)\mathrm{d}\eta\right)\right]\mathrm{d}r\right\} \tag{9}$$

For the case in which $\varepsilon^{c}(r) = \varepsilon^{c}$ is independent of r, (9) becomes:

$$\Delta\sigma_{rr}(R) = 2\mu\varepsilon^{c}\left[2\ln\left(\frac{R}{R_s}\right) - \frac{2}{3}\left(1 - \left(\frac{R_s}{R}\right)^{3}\right)\right] \tag{10}$$

Now let $R_s = R - h$ and expand (10) in small h/R to obtain:

$$\Delta\sigma_{rr}(R) = 2\mu\varepsilon^c\left(\frac{h}{R}\right)^2 + \ .....\tag{11}$$

By (11), creep affects the stresses in the TBC only to order $(h/R)^2$. While there is no reason to expect that the creep strain distribution through the TGO should be uniform: nevertheless, the above result strongly suggests that creep in the TGO will have minimal influence in relaxing the stresses in the TBC. (This conclusion must again be tempered by the limitations of the spherical imperfection model). Conversely, the deviatoric component of the stress in the TGO itself could relax, resulting in a reduction in the hoop stress (for compatibility reasons, the radial stress would be unaffected).

2.4. Cracking scenario

2.4.1. Crack patterns

The preceding distributions of tensile stress may be used to infer cracking patterns. These motivate the explicit fracture mechanics problems to be solved. They are validated by the solutions. The hoop tensions induced in the TBC as the TGO thickens would allow radial cracks to form (Fig. 6a). These are analyzed in Section 2.4.2. Such cracks would not be expected to penetrate back through the TGO, even though it is subject to hoop tension, because creep redistributes the concentrated stresses at the inner crack front (A in Fig. 6a). Subsequent cooling to ambient enhances the hoop tensions in the TBC (Fig. 4**B**), but diminishes the radial compressions normal to the interface between the TGO and the bond coat. Moreover, should the growth stresses be sufficiently relaxed by bond coat creep, then, at ambient, these stresses may be tensile. In either case, upon cooling, the radial crack in the TBC could extend from its inner front, through the TGO, and along the interface, to create a fully-connected radial crack (Fig. 6c). Solutions for such crack configurations are presented in Section 2.4.3. Since the formation of such a configuration requires that the crack penetrate the TGO, which is in hoop compression at ambient, it is surmised that this happens upon thermal cycling at temperatures wherein the TGO is brittle (below about 900C) yet the hoop stresses are still tensile (Fig. 6b).

2.4.2. Cracking in the TBC

Prior to cracking, the largest tensile hoop stresses in the TBC occur at temperature due to growth. From (4b), this stress is

$$\sigma_{\theta\theta} = \sigma^*\left(\frac{R}{r}\right)^3\tag{11a}$$

where

$$\sigma^* = \frac{E(m-1)}{3(1-\nu)m}\left(\frac{h}{R}\right)\tag{11b}$$

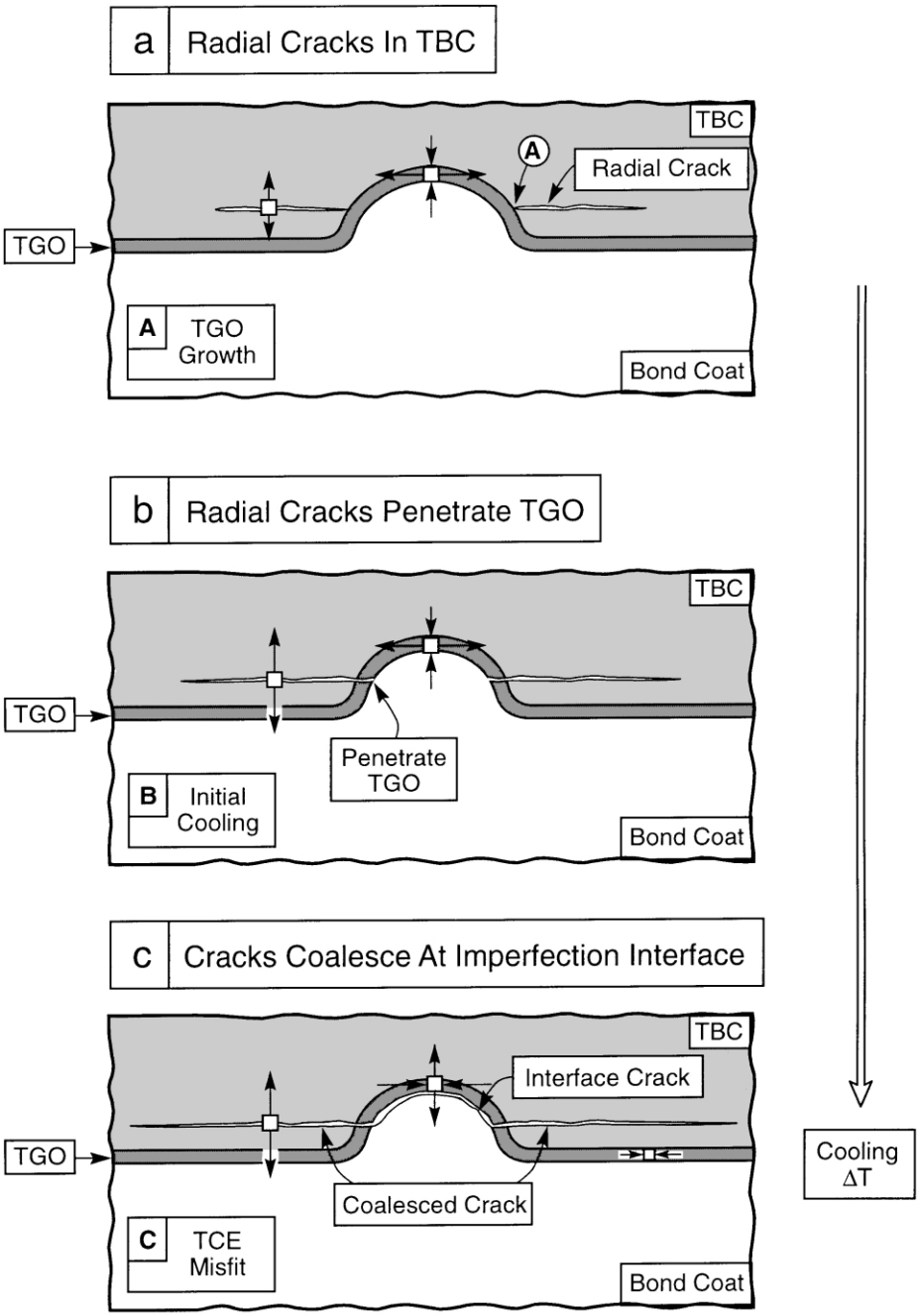

Fig. 6. Cracking patterns expected around imperfections as a result of the stress distribution (see Fig. 2b). The actual incidence of cracks depends on variables such as the TGO thickness, the imperfection diameter and the TBC toughness.

is the hoop stress in the TBC at the interface with the TGO. Shum and Huang [38] have presented results relevant to such a stress state for a configuration comprising an equatorial ring crack with inner radius R and outer radius a. The following are analytical expressions for the stress intensity factors at the inner and outer crack edges (which have been fitted to their numerical results) [38]:

$$\frac{K}{\sigma^*\sqrt{R}} = \sqrt{\frac{\pi}{2}\left(\frac{a}{R}-1\right)}\left(\frac{R}{a}\right)^{2.4} \qquad \text{(outer crack edge)} \tag{12a}$$

$$\frac{K}{\sigma^*\sqrt{R}} = \sqrt{\frac{\pi}{2}\left(\frac{a}{R}-1\right)}\left(\frac{R}{a}\right)^{0.55} \qquad \text{(inner crack edge)} \tag{12b}$$

These results are plotted in Fig. 7a. Note the very large stress intensity at the inner front. It is this intensity that motivates the crack to penetrate the TGO and coalesce along the interface (Fig. 6c) as the system thermally cycles. Eqs. (12a) and (12b) apply to the case of no elastic mismatch, but Shum and Huang [38] also present results for a full range of elastic mismatch between the inner spherical region, $r < R$, and the outer region, $r \geqslant R$. When applied to the present problem (Table 1), (12a) underestimates K by about 30%, with E in (11b) identified with the modulus of the TBC. As a representative example, consider a TBC with $E = 30$ GPa and $K_{\mathrm{Ic}}^{\mathrm{tbc}} = 0.5$ MPa $\sqrt{\mathrm{m}}$ [39–41] and an imperfection with $R = 20$ μm, $h/R = 1/10$ [41] and $m = 1.3$. If an equatorial crack were initiated at the imperfection, (12) predicts it would expand outward to a radius about three times R. Evidently, further increases in h/R (with greater exposure time) would cause the crack to continue expanding. Note from the plot in Fig. 7a that the same value of K is attained for a very small initiating crack, and thus there would appear to be only a very small barrier to the initiation of an equatorial crack in the TBC.

2.4.3. Cracking in the TBC and the TGO with debonding of the TGO/bond coat interface

It has just been demonstrated that the imperfection induces significant hoop tension in the TBC due to TGO growth, which can give rise to a substantial TBC crack at the growth temperature. Cyclic temperature variations may cause it to become fully connected and enlarge it further. A model for estimating the stress intensity factor at the outer edge of the fully cracked configuration is constructed as follows (neglecting elastic mismatch effects). The complete solution for a full circular crack, radius a, with faces subject to a uniform normal opening pressure p extending from the center out to radius R is given by Tada, Paris and Irwin [42]. The pressure p is identified by equating the opening displacement at the center of the crack with the wedge opening, $2(m-1)h/m$. The resulting stress intensity factor is [42]:

$$\frac{K}{\sigma^*\sqrt{R}} = \frac{3}{2(1+\nu)}\sqrt{\frac{\pi}{2}\frac{R}{a}}\left[1+\frac{(R/a)\cos^{-1}(R/a)}{1-\sqrt{1-(R/a)^2}}\right]^{-1} \tag{13}$$

This result is plotted in Fig. 7b for $\nu = 1/3$. Note that, for larger values of a/R, (13) asymptotes to:

$$\frac{K}{\sigma^*\sqrt{R}} = \frac{3}{2(1+\nu)\sqrt{\pi}}\left(\frac{R}{a}\right)^{3/2} \tag{14a}$$

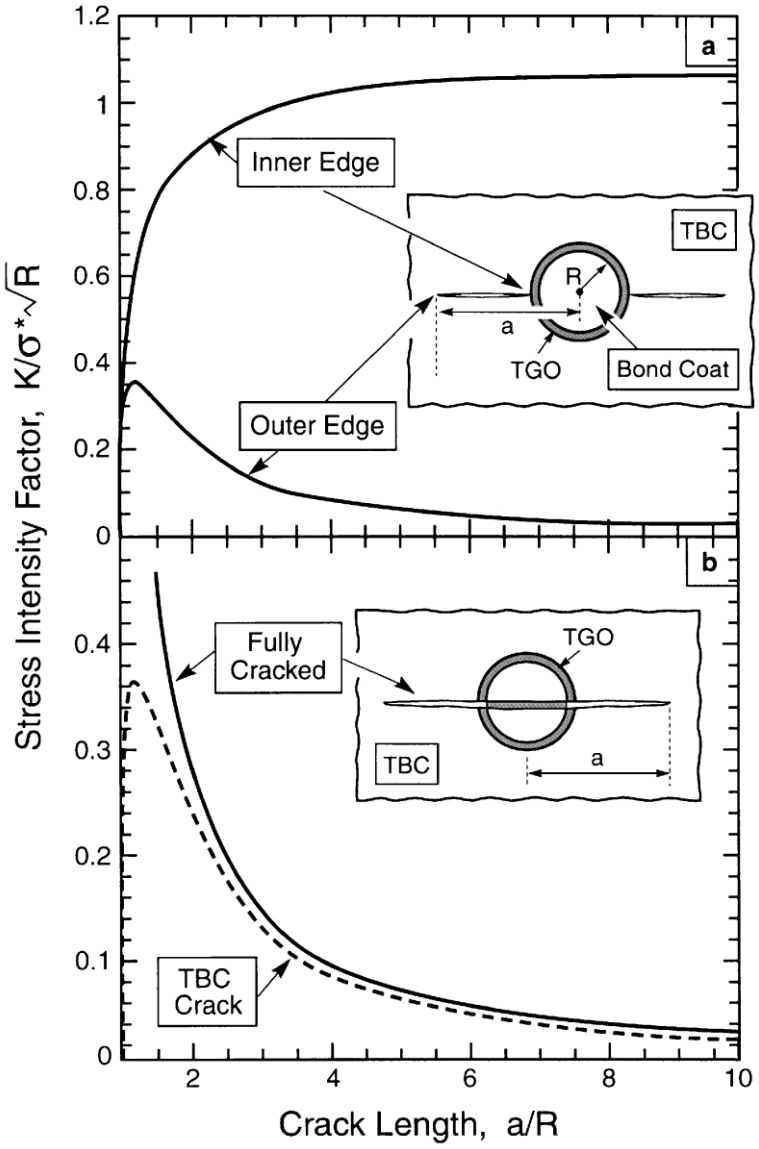

Fig. 7. Stress intensity factors calculated for the crack configurations depicted on the insets.

while (12a) asymptotes to

$$\frac{K}{\sigma^*\sqrt{R}} = \sqrt{\frac{\pi}{2}}\left(\frac{R}{a}\right)^{1.9} \tag{14b}$$

Over the range of a/R from 2 to 10 plotted, there is little difference between these results. Accordingly, the principal role of thermal cycling is to cause the inner front of the crack in the TBC (induced by the growth misfit) to penetrate back through the TGO, and along the interface, to form a fully-connected crack. In this configuration, the crack can coalesce with others to form a separation zone large enough to satisfy large scale buckling requirements, discussed next.

2.5.2. Coalescence

The mechanics of crack coalescence in residually stressed films are subject to nuances associated with remnant ligaments that arise because the energy release rates approach zero at convergence [43]: whereupon the ligaments can only be detached by applying a (small) transverse force [43]. With the simplifying assumption that such forces are always present (because of inertial effects or vibration), crack coalescence can be ascribed to a requirement that the crack diameter equal the spacing 2d between neighboring imperfections. With this simplification, (14a) can be re-expressed as a failure criterion. That is, fracture occurs at a critical TGO thickness, h_c, given by:

$$h_c = \frac{2\sqrt{\pi}(1-\nu^2)md^{3/2}K_{Ic}^{tbc}}{(m-1)RE_{tbc}} \tag{15}$$

Note the key role of imperfections, through their diameter $2R$, and the spacing, $2d$. Moreover, since h_c depends on time-at-temperature t ($h = \sqrt{D_{ox}t}$), then (15) can be re-expressed as a failure time. It is to be appreciated that D_o is a strong function of temperature and that K_{Ic}^{tbc} is sensitive to the TBC microstructure. Accordingly, this formula (15) can be used as the basis for durability models.

3. Numerical results

With the above assessment providing guidelines for the scaling as well as approximate magnitudes for the stresses and the TBC crack sizes, some selected numerical results have been obtained for imperfections having more realistic morphologies and for the explicit constituent properties indicated on Table 1. The imperfections are taken to have a cosine shape (Fig. 8) and the stresses are calculated with the finite element method using the ABAQUS code. It will be shown that the stresses induced by both thermal expansion misfit and growth have the same form as those anticipated by the analytical model, especially in the region around the apex of the imperfection.

3.1. Thermal expansion misfit

The stresses absent a TGO, upon cooling to ambient, are summarized on Fig. 8b and c (results for $h/L = 0$). Note that there are σ_{nn} tensile stresses at the interface around the undulation peaks, with a maximum at the apex. There are also σ_{zz} tensile stresses in the

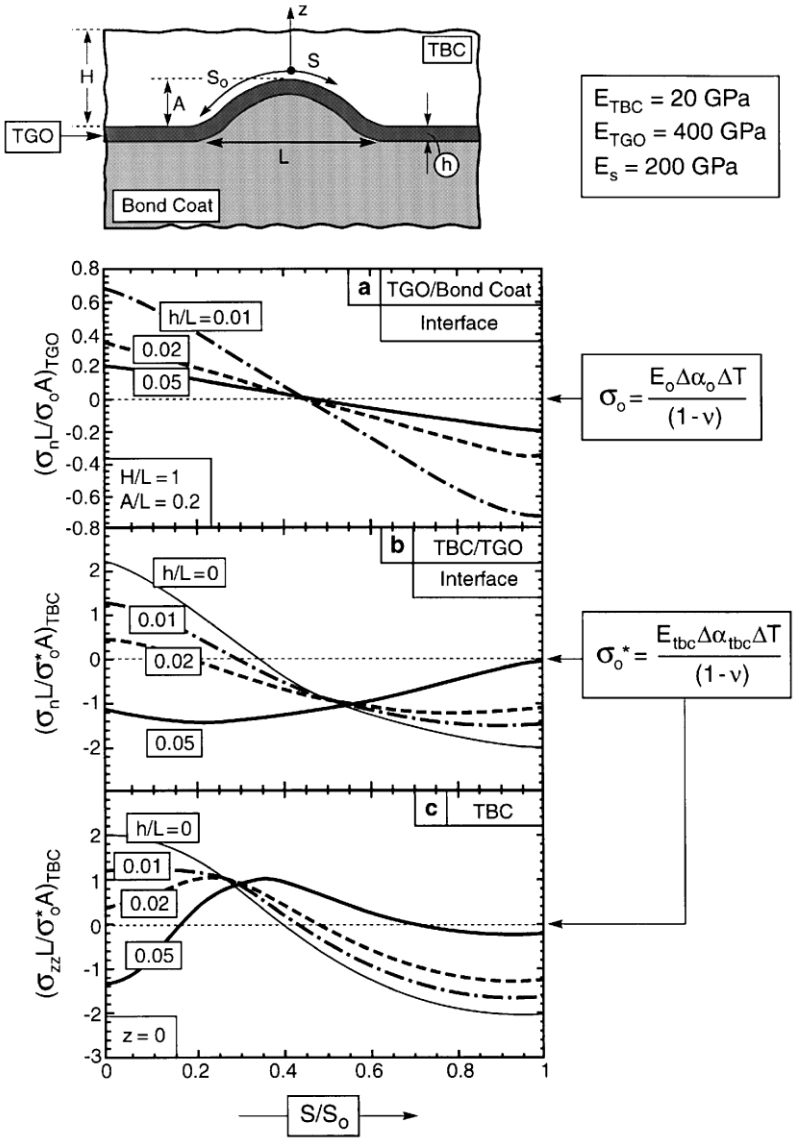

Fig. 8. The effect of TGO thickness, h/L, on the thermal expansion misfit stresses in the vicinity of a sinusoidal imperfection. (a) The normal stresses at the TGO/bond coat interface, normalized by σ_o. (b) The normal stresses at the TGO/TBC interface normalized by σ_*. (c) The σ_{zz} stress in the TBC normalized by σ_*.

TBC around the apex. The magnitudes are relatively small because of the compliance of the TBC.

The influence of the TGO on these stresses is crucial, since failure is known to be dependent on the TGO thickness. In order to separate the response on cooling from that during growth, the TGO has been introduced at the growth temperature and

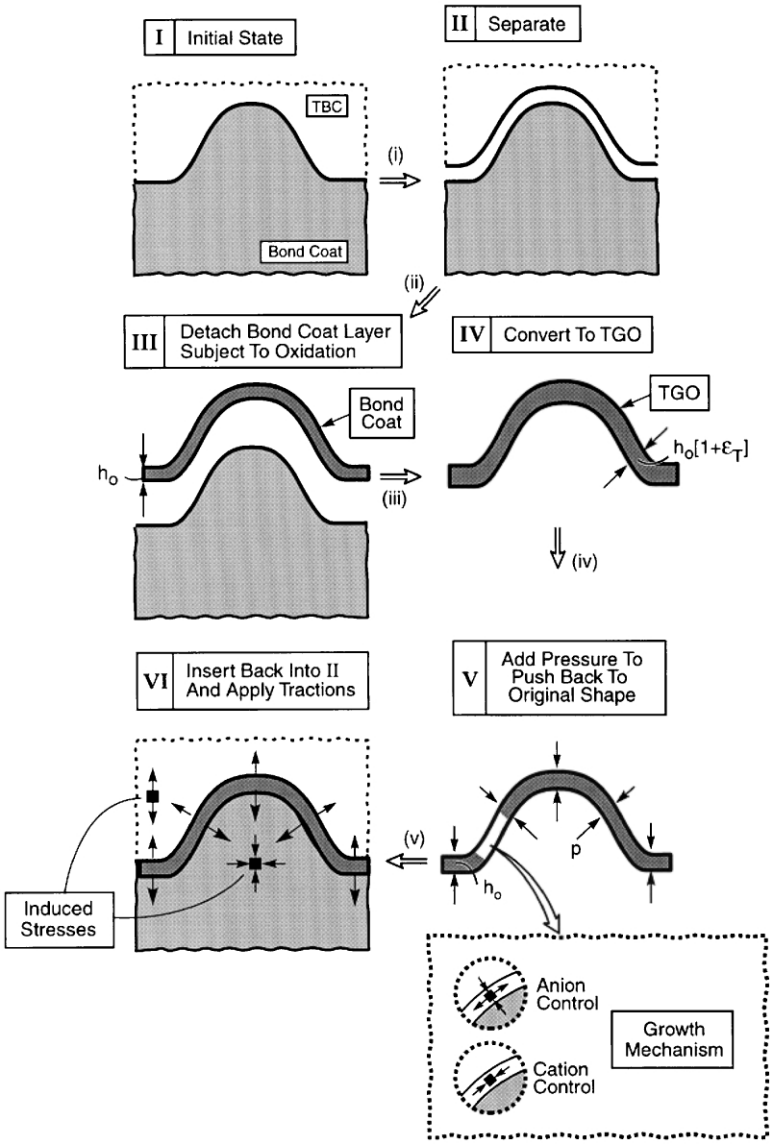

Fig. 9. A schematic of the Eshelby protocol used to calculate the growth stresses around an imperfection by using the finite element method.

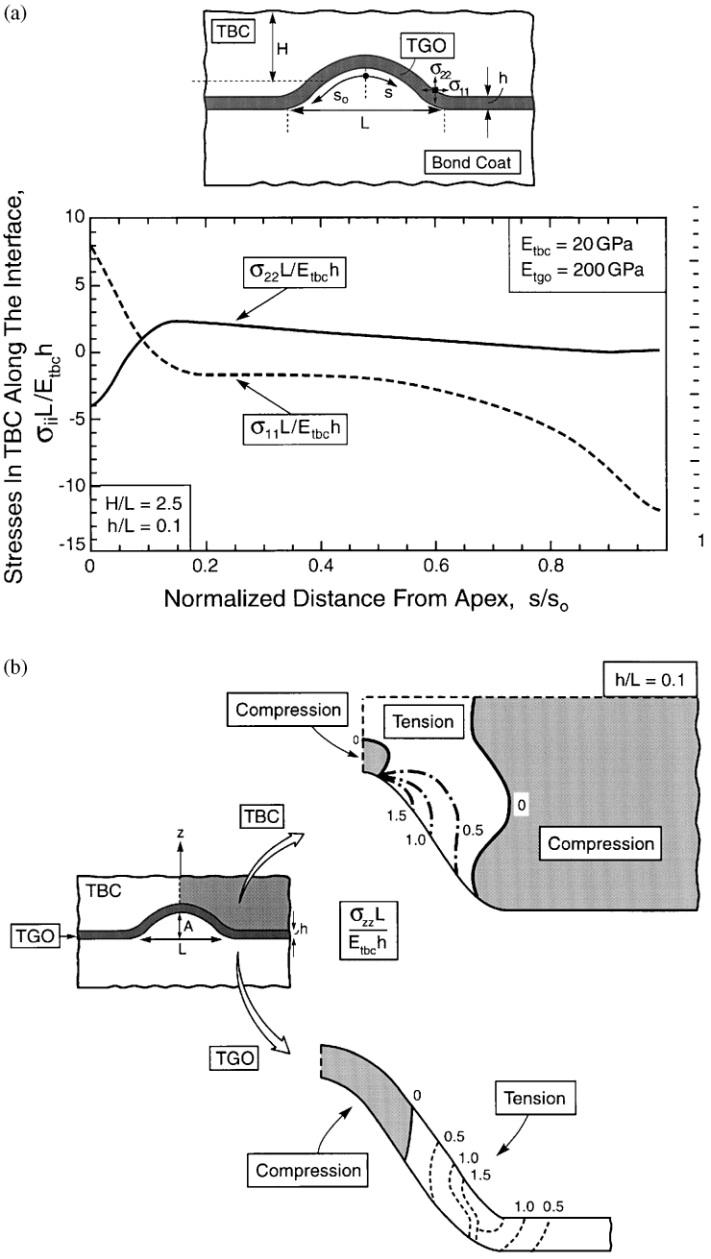

Fig. 10. Numerical results for the stress induced by anion-controlled TGO growth. (a) The σ_{zz} and σ_{xx} stress distributions along the TBC/TGO interface. (b) Contours of the σ_{zz} stresses in the TBC and TGO.

assumed to be stress-free. That is, growth stresses and strains are added-in later by superposition. The effect of the TGO on the σ_{zz} tensile stress distribution around the imperfections is shown on Figs. 9a–c (results for $h/L > 0$). The three main features of the stress near the apex are consistent with the analytical model.

(i) There is a tensile stress normal to the TGO/bond coat interface (Fig. 8a), but it decreases somewhat as the TGO thickens.
(ii) The stress at the TGO/TBC interface is initially tensile, but becomes compressive when the TGO thickness exceeds about $h/L = 0.03$ (Fig. 8b).
(iii) A zone of σ_{zz} tension develops in the TBC at the sides of the imperfection as the TGO thickens (Fig. 8c).

3.2. Growth stresses

The relative magnitudes of the stresses that develop during TGO growth are again determined by the Eshelby protocol (Fig. 9). For this purpose the following two problems are solved using the finite element method.

(i) Problem I. The interface between the TBC and bond coat is opened so that the new TGO can form in an unconstrained manner. Tractions, p, are calculated sufficient to push the TGO into the volume originally occupied by the bond coat before it was oxidized.
(ii) Problem II. The TGO is inserted back into the overall system to create the two new interfaces (TBC/TGO and TGO/bond coat), whereupon equal and opposite tractions, $-p$, are applied to regain equilibrium.

The final stress field is the sum of those induced in both steps. This process commences with a small initial thickness of TGO, the stresses are calculated and the process repeated multiple times to simulate the growth.

The results of one such calculation for anion-controlled TGO growth are summarized in Fig. 10a and b. Note that the σ_{zz} stresses have the same form as those assessed using the analytical model. Namely, the TBC just outside the TGO experiences tensile σ_{zz} stress over the full imperfection domain (Fig. 10a). The extent of the tensile zone is depicted on figure 10b. There is also σ_{zz} tension over a substantial portion of the TGO, along the sides of the imperfection (Fig. 10b). These σ_{zz} stresses allow radial cracks to form in the TBC as the TGO thickens (Fig. 6a).

4. Concluding remarks

Straightforward methods of analysis have been used to derive relationships that characterize the failure of TBCs. It is proposed that these relationships be used as scaling laws that predict trends with key variables and also rationalize experimental measurements. One of the basic findings is that (in accordance with practical experience) a critical TGO thickness, h_c, is needed to cause failure. Through the

present scaling laws, h_c can be related to underlying microstructural and morphological features present in the TBC system (15). This critical thickness can be related to the durability through the growth kinetics of the TGO. It remains to validate these predictions through a critical set of experimental measurements. Subject to validation, a future goal would be to use the scaling results to suggest directions for increasing the critical thickness and, thereby, enhancing durability.

It is reiterated that the scenario considered here is one involving minimal thermal cycling, whereupon ratcheting of the TGO is excluded as a major source of the σ_{zz} stress. When ratcheting conditions are created, the scaling laws change dramatically, as discussed elsewhere [27].

References

[1] Miller RA. J Am Ceram Soc 1984;67:517.
[2] Mariochocchi A, Bartz A, Wortman D. Thermal barrier coating workshop, NASA CP 3312, 1995. p. 79.
[3] Bose S, DeMasi-Marcin J. Thermal barrier coating workshop, NASA CP 3312, 1995. p. 63.
[4] DeMasi-Marcin JT, Gupta DK. Surf Coatings Technol 1994;68/69.
[5] Hillary R, editor. NRC Report. Coatings for high temperature structural materials, National Academy Press, 1996.
[6] Strangman TE. Thin Solid Films 1985;93–105:127.
[7] Meier SM, Gupta DK. Trans ASME 1993;116:250–7.
[8] Wright PK, Evans AG. Current Opinion in Solid State and Materials Science 1999;4:255–65.
[9] Wright PK. Mater Sci Eng 1998;A245:191–200.
[10] Kingery WD, Bowen HK, Uhlmann DR. Introduction to ceramics. Wiley and Sons, New York (1976): Nicholls JB, Lawson KJ, Rickerby DS, Morell P. AGARD Report R-823, April 1998.
[11] Golightly FA, Stott FH, Wood GC. Oxid Metals 1976;10:163.
[12] Stiger MJ, Yanar NM, Topping MG, Pettit FS, Meier GH. Z Metallk 1999;90:1069–78.
[13] Quadakkers WJ, Tyagi AK, Clemens D, Anton R, Singheiser L. In: Hampikian JM, Dahotre NB, editors. Elevated temperature coatings: science technology. Warrendale, PA: TMS, 1999. p. 119.
[14] Smeggil JG. Mater Sci Eng 1987;87:261–5.
[15] Smialek JL, Jayne DT, Schaeffer JC, Murphy WH. Thin Solid Films 1994;253:285–92.
[16] Smialek JL, Tubbs BK. Metall Mater Trans 1995;A26:427.
[17] Lipkin DM, Clarke DR. Oxid Metals 1996;45:267–80.
[18] Tolpygo VK, Clarke DR. Oxid Metals 1998;49:187–211.
[19] Christensen R, Lipkin DM, Clarke DR, Murphy K. Appl Phys Lett 1996;69:3754–6.
[20] Sergo V, Clarke DR. J Am Ceram Soc 1998;81:3237–42.
[21] Choi SR, Hutchinson JW, Evans AG. Mech Mater 1999;31:431–47.
[22] Meier SM, Nissley DM, Sheffler KD. Thermal barrier coating life prediction model development — phase II, NASA CR-18911, July 1991.
[23] He MY, Evans AG, Hutchinson JW. Mater Sci Eng 1998;A245:168–81.
[24] He MY, Evans AG, Hutchinson JW. Acta Mater 1997;45:3481–9.
[25] Tolpygo VK, Clarke DR. Acta Mater 1998;46:5153–66.
[26] Gell M, Vaidyanathan K, Barber B, Cheng J, Jordan E. Metall Mater Trans 1999;30A:427.
[27] He MY, Evans AG, Hutchinson JW. Acta Mater, 2000;48:2593–601.
[28] Rhines FN, Wolf JS. Metall Trans 1970;1:1701–10.
[29] Dove DB, Baldwin D. H Metall Trans 1974;5:1637–41.
[30] Eshelby JD, Proc R. Soc 1957;A241:376.
[31] Evans AG, He MY, Hutchinson JW. Acta Mater 1997;45:3543–54.
[32] Tolpygo VK, Clarke DR. Acta Mater 1998;46:5167–74.

[33] Tolpygo VK, Dryden J, Clarke DR. Acta Mater 1998;46:927–37.
[34] Cannon RM, Rhodes WH, Heuer AH. J Am Ceram Soc 1980;63:46.
[35] Heuer AH, Tighe NJ, Cannon RM. J Am Ceram Soc 1980;63:53.
[36] Cho J, Harmer MP, Chan HM, Rickman JM, Thompson AM. J Am Ceram Soc 1997;80:1013.
[37] Fang J, Thompson AM, Harmer MP, Chan HM. J Am Ceram Soc 1997;80:2005.
[38] Shum DKM, Huang YY. Eng Fract Mech 1990;37:107–17.
[39] Johnson CA, Ruud JA, Bruce R, Wortman D. Surf Coatings Technol 1998;108/109:80.
[40] Choi SR, Zhu D, Miller RA. Ceram Eng Sci 1998;19:293–301.
[41] Rabiei A, Evans AG. Metall Mater Trans, 2000;48:3963–76.
[42] Tada H, Paris PC, Irwin GR. Handbook for stress analysis of cracks, 2nd ed. Del Research, 1985 — to be reissued by the American Society of Mechanical Engineering.
[43] Evans AG, Hutchinson JW, He MY. Acta Mater 1999;47:1513–22.